JOURNAL OF PROPULSION AND POWER
Vol. 23, No. 1, January–February 2007

Laser Propulsion for Ground Launch

David P. Resendes,* Sérgio Mota,† and José T. Mendonça‡
Instituto Superior Técnico, 1049-001 Lisbon, Portugal
Berry Sanders§
TNO Prins Maurits Laboratory, 2280 AA Rijswijk, The Netherlands
João Encarnação‖
Delft University of Technology, 2600 AA Delft, The Netherlands
and
Jose Gonzalez del Amo¶
ESA, 2200 AG Noordwik, The Netherlands

DOI: 10.2514/1.24527

Ground-to-orbit launch using laser propulsion requires a thermal system. A number of such thermal thruster concepts have been developed in the past. Thus far, only the laser-supported detonation thruster concept has led to a flight vehicle, the Lightcraft. It is shown via flight simulations and measurements with the Lightcraft that there are no inherent limitations for a ground-to-orbit launch vehicle using laser propulsion. A planar geometry laser-supported detonation thruster using a CO_2 laser is considered and its performance evaluated. A 10-km height flight vehicle using existing lasers is proposed.

Nomenclature

A	=	area
C_a, C_n	=	drag coefficients
F	=	force resultant, thrust
g_0	=	surface gravitational constant
h	=	specific enthalpy of gas, height
h_P	=	Planck's constant
h_{lsr}	=	laser site altitude
h_{ref}	=	atmospheric scale height
I_{abs}	=	laser intensity absorbed by gas
I_{sp}	=	specific impulse
k	=	absorption coefficient
k_B	=	Boltzmann's constant
m	=	mass
$\dot{m}$	=	mass flow rate
n_X	=	number density of X
P	=	power
p	=	pressure
q	=	specific heat added to gas
r	=	radius
$r_{\text{hot spot}}$	=	vehicle hot-spot radius
r_{lsr}	=	laser main deflector radius
T	=	temperature
u	=	velocity in shock-fixed reference frame
v	=	velocity in laboratory reference frame
α_{abs}	=	atmospheric absorption coefficient
ΔR_{slant}	=	slant range
η	=	efficiency
θ	=	semivertex angle
Λ	=	longitude
λ	=	wavelength
ρ	=	density
υ	=	laser frequency
Φ	=	latitude
Ω_e	=	Earth's rotational velocity

Presented at the 41st AIAA/ASME/SAE/ASEE Joint Propulsion Conference and Exhibit, Tucson, AZ, 10–13 July 2005; received 9 April 2006; revision received 11 April 2006; accepted for publication 12 April 2006.

*Professor, Physics; resendes@ist.utl.pt. AIAA Associate Fellow.
†Ph.D. Student, Physics; smota@ist.utl.pt.
‡Full Professor, Physics; titomend@ist.utl.pt.
§Project Manager, System Performance and Survivability Department; sanders@pml.tno.nl.
‖Ph.D. Student, Aerospace; joao.encarnacao@mail.telepac.pt.
¶Head, European Space Research and Technology Center, Electric Propulsion Section; jose.gonzalez.del.amo@esa.int.

I. Introduction

LASER propulsion allows for the possibility of rockets with high specific impulse (I_{sp}), high thrust, and low propulsion weight, a combination of advantages not apparent in any other rocket propulsion scheme. Laser-heated rockets have the potential for producing more than 1000 s of I_{sp}, by heating the propellant to more than 4000 K. The thrust depends on the power that can be absorbed in the propellant, and this is only limited by the laser power available at the rocket. Because laser power can be beamed from a remote laser source, a laser-heated rocket need not carry its power source, enabling low weight.

The simplest propulsion system that accomplishes this consists of a solid propellant, the surface of which is continuously being vaporized by laser irradiation. To increase the specific impulse and still preserve the steady-state nature of the flow, it is necessary to volumetrically add significant energy directly to the vapor. While the implementation of the thruster configuration may assume different forms, thermal laser propulsive concepts are based on absorption in a laser-supported combustion (LSC) wave or in a laser-supported detonation (LSD) wave. Independently of the ignition mechanism, these waves are sustained by inverse Bremsstrahlung (IB) absorption. In IB absorption, the laser energy is converted directly to gas translational energy during the (high-temperature) spectrally continuous absorption process. Handling the resulting hot gases poses two related problems: 1) the gas must be confined without damage to the walls by the heat load; and 2) the heat losses must be minimized. Based on thermodynamic constraints, only the subsonic LSC wave could be used efficiently in a converging–diverging nozzle. The supersonic LSD wave can only be efficiently implemented in a diverging nozzle configuration.

Steady laser-heated LSD wave flows using LiH as propellant have been modeled assuming chemical equilibrium. The resulting structure of the LSD waves has been derived. Thruster performance calculations for the equilibrium LiH model are obtained.

Thermodynamic equilibrium is assumed as this is the relevant equilibrium over the hydrodynamic time scale of interest.

Numerical simulations were performed to gain insight into the flight mechanics analysis of laser propulsion ascent trajectories and how these are influenced by the most relevant mission parameters. COLVET, a launch vehicle simulation tool, also capable of simulating the motion of laser-propelled vehicles, was used for this purpose. Experimental data from a laser-propelled flight were used to reproduce the experiment with the simulation tool. This exercise proved to be extremely useful, because it provided insight into the physical constraints that are most significant in laser propulsion motion.

Our objective in this paper is to discuss in a nonintegrated way modeling aspects of thermal laser absorption and ascent trajectories, both related to areas of laser-powered ground launch. The emphasis is on an overview presentation and an evaluation of feasibility of launches of up to a few kilometers using existing CO_2 laser technology. The current launch altitude record stands at 71 m. In Sec. II, the ideal performance for a laser thruster is defined. In Sec. III, the physical mechanisms involved are briefly reviewed. Section IV presents the results of steady one-dimensional planar flow in a channel. Section V discusses flight simulations including comparison with Lightcraft measurements. The final section presents our conclusions.

II. Ideal Performance

In a thermal laser propulsion system, thrust is produced by converting the energy from a laser beam into random kinetic energy of a working fluid and then expanding this heated fluid through a propulsive nozzle. Rocket performance is characterized by thrust and specific impulse. The (instantaneous) thrust is the reaction force associated with the momentum flux of propellant, $F = \dot{m}v_e$, where $\dot{m}$ is the rate at which mass flows out of the chamber and v_e is the mass averaged exhaust velocity. Specific impulse gives the impulse delivered per unit weight of ejected propellant, $I_{\text{sp}} = \dot{m}v_e/\dot{m}g = v_e/g$, where g is the gravitational constant. Under ideal conditions, the power in the laser beam is completely converted to kinetic power in the propellant, $P_G = \frac{1}{2}\dot{m}v_e^2$. Thus, the ideal performance potential of a laser-powered propulsion system, determined under the assumption of complete conversion of laser energy into directed propulsive energy, is given by the following relations:

$$F = \sqrt{2P_G\dot{m}} \tag{1}$$

$$I_{\text{sp}} = \frac{\sqrt{2}}{g}\sqrt{\frac{P_G}{\dot{m}}} \tag{2}$$

To obtain these relations, the kinetic power is solved for v_e and the result substituted in the respective definitions. From these relations, it is clear that propulsive performance depends only upon the mass flux and the rate at which heat is added to the working fluid. For a fixed laser coupling efficiency and for continuous wave (CW) laser operation, only one of P_G and $\dot{m}$ is independent, although this is not apparent from these relations. Indeed a particular intensity level, and a corresponding particular total laser power, will define a unique mass flow rate.

These relations can be inverted to express the flow rate and thrust of an ideal rocket in terms of the specific impulse I_{sp}, as shown in Fig. 1. This plot serves to emphasize the large powers involved in high I_{sp} rockets. A thrust of 1000 N at an I_{sp} of 2000 s has 10 MW in the exhaust and requires 0.05 kg/s of mass flow. This may be interpreted as the specific enthalpy to which the propellant gas must be heated, which can be converted to kinetic temperature when the gas and pressure are specified. For the example given, the propellant specific enthalpy is 200 MJ/kg. This value is to be contrasted with typical chemical values, of the order of 5 MJ/kg. To achieve high performance, the reduced mass flow rate must be compensated by a high specific enthalpy. Clearly, such high average power lasers are not yet available although some designs exist [1]. The current laser

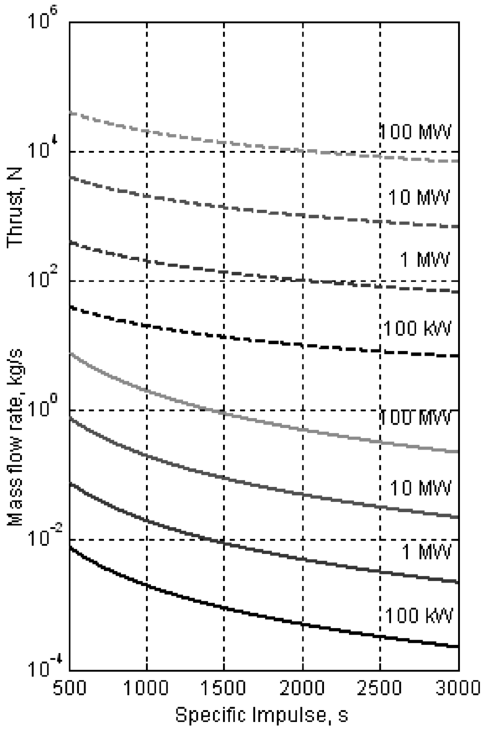

Fig. 1 Ideal laser rocket performance.

technology applicable to laser propulsion is roughly 100 kW average power at 10.6 μm wavelength (CO_2 laser). Thus, at least in the near term, launching of small launch vehicles, on the order of 1 kg, should be the main application of laser propulsion.

The actual performance of a propulsive system is subject to losses that, although straightforward to enumerate, are difficult to calculate. These losses include transmission losses between the laser source and the receiving "optics" on the propulsive vehicle, losses in the optical system, losses because of incomplete absorption of the radiant energy in the working fluid, and losses from the fluid after the radiation has been absorbed. Losses have a multiplicative effect on the amount of energy that is required to reach a given specific impulse. Because of the large average powers involved for interesting payloads and the relatively slow time scale for hydrodynamic fuel ejection as compared to absorption processes, it is clear that in a ground-to-orbit application, the dominant physical power transfer mechanism must be thermal.

III. Overview of Thermal Thruster Physics

In a laser thruster, the absorption of laser radiation is coupled to the propellant flow. The simplest description of heat addition by absorption of radiation is a constant area, one-dimensional flow. Although this description is far from the configuration in a propulsive application, it provides insight and qualitative understanding. As in the case of one-dimensional combustion of a premixed fuel/oxidizer combination, the problem of heat addition by absorption of radiation can have two solutions: a subsonic solution (deflagration or combustion branch), and a supersonic solution (detonation branch) [2]. Although the implementation of the thruster configuration may assume different forms, thermal laser propulsive concepts with high specific impulse are based on one of these solutions. Steady subsonic flow in an adiabatic, variable-area channel is possible in a converging nozzle or a diverging diffuser, whereas steady supersonic flow is possible in a diverging nozzle or a converging diffuser. Based on thermodynamic constraints imposed by the energy equation for an adiabatic nozzle and the requirement of isentropic flow, only the subsonic LSC (combustion) wave could be used efficiently in a converging–diverging nozzle. The supersonic LSD (detonation) wave can only be efficiently implemented in a diverging nozzle configuration. The geometry of the thruster itself cannot be

determined based on thermodynamics alone; fluid mechanics is required.

Thermodynamic constraints limit the LSC wave mechanism to the converging–diverging nozzle configuration with laser absorption in the converging part. This configuration requires careful focusing through a throat in the single port configuration (absorption and exhaust channel are the same) or the use of two ports, one for admission of the laser in the converging portion by means of some focusing mirror, and a separate exhaust in the diverging portion. In addition, for constant thrust a CW laser should be used [3,4]. CW LSC (as well as CW LSD) absorption is, however, hydrodynamically unstable for the greater part of the parameters of interest and is therefore not robust [5]. A pulsed laser is to be preferred. Using a pulsed laser, propulsion based on the LSC mechanism is more complicated and less efficient than the use of the pulsed LSD mechanism, as will be argued later. Additionally, the pulsed LSD wave mechanism, which can be implemented in the diverging nozzle configuration, is far simpler from a hardware point of view.

Laser-supported detonations may be initiated either by direct or by indirect means. In direct initiation, a sufficient amount of energy is deposited rapidly in the propellant resulting in the emergence of a detonation after an initial adjustment period. A simple criterion for direct initiation is that the energy deposited be sufficient to maintain a shock at least as strong as the leading shock of a Chapman–Jouguet (CJ) wave for a time period at least as long as the energy deposition time. In indirect initiation, the ignition source is weaker and produces a deflagration that subsequently undergoes a transition to a detonation. The buildup of pressure waves assumes an important role in promoting this transition, which is facilitated by confining the mixture. Pirri studied the LSC to LSD wave transition above metal surfaces at atmospheric pressure [6]. At intensities slightly higher than plasma threshold (exponential electron increase), a laser-supported combustion wave is usually ignited. LSC waves are often seen at intensities from $(2 \times 10^4$–$10^6)$ W/cm^2 for 10.6 μm radiation with both CW and pulsed laser beams. The ignition of a LSC wave initially takes place in the vapor [7,8]. The heated target vapor subsequently transfers its energy to the surrounding air. Once the air begins to absorb a significant fraction of the laser energy, the LSC wave propagates into the air along the beam path. As a consequence of the ignition process and the presence of the target surface, a precursor shock precedes the LSC wave, except at the lowest intensities. A LSC wave propagates into shocked air at very low velocity and thus the absolute wave velocity approximately equals the particle velocity behind the shock. The pressure throughout the region between the wall and the precursor shock remains approximately constant. Because the mass flow through the LSC wave is very low, the plasma temperature is high, leading to strong radiation loss from the plasma.

When the laser intensity is increased, the wave velocity becomes greater than the particle velocity behind the shock because the radiative transfer and the higher temperatures behind a stronger shock result in higher LSC wave speeds. This may be called the weak LSD wave regime where the pressure decreases across the LSC wave. The wave speed relative to the particle speed continues to increase as the laser intensity is increased until the relative particle velocity behind the LSC wave becomes sonic (the Chapman–Jouguet point). The absorption zone now has a velocity equal to the shock velocity and the conditions behind the narrow absorption zone are given by classical LSD wave theory. The laser beam absorption occurs in a thin zone of hot, high-pressure gas behind the shock wave.

It is found that the maximum energy transfer per unit area transmitted to a surface behind the vapor is obtained when a slowly propagating LSC wave plasma is ignited behind a strong precursor shock in one-dimensional geometry. The pressure is high and so is the temperature because the absolute wave velocity approximately equals the particle velocity, and so the mass flow through the LSC is small. The radiation from the plasma is maximized under these conditions. These conditions all favor low propulsion efficiency. When the transition to the LSD wave begins, the mass flow through the absorption zone increases, and increasing the laser intensity further simply partitions more energy into a higher mass flow. The wave propagates faster, but the energy transfer to the surface does not increase. When an LSD wave configuration is ignited, the temperature may actually be lower than for the LSC wave case because the wave is propagating at a higher velocity. Thus, in the presence of a surface, the LSD mechanism is superior to the LSC mechanism for a propulsion application.

In a typical pulsed laser thruster [9], the absorption of laser radiation is initiated by focusing the incoming laser beam to produce a laser-induced breakdown of the working fluid just downstream of a nozzle throat, or at the focus of a diverging nozzle. The resulting high-pressure plasma continues to absorb laser energy, generating a moving LSD wave. The LSD wave propagates along the beam path and expands down the nozzle. With a short laser pulse, the LSD wave quickly becomes a blast wave that propagates to the nozzle exit plane, converting the high pressure of the propellant gas behind it into a force on the nozzle walls to create thrust. To absorb the laser energy efficiently, the induction time to achieve breakdown should be short compared to the laser pulse duration, and the resulting plasma should be opaque to the laser energy.

LSC and LSD absorption is maintained by IB [10]. IB is a broadband mechanism in which electrons interact with ions or atoms to absorb laser energy at any wavelength, but with a wavelength dependence that makes absorption at longer wavelengths more favorable. Once the initial electron production is achieved, the LSC or the LSD absorption mechanisms maintain the working fluid at ionization temperatures. The flow rate and size of the wave dictates the amount of gas processed, and the efficiency of the processing and expansion through the nozzle dictate the engine performance. The initial electron population itself may grow continuously (continuous absorption) or abruptly as a sudden flash (laser-induced breakdown).

We conclude this brief overview by addressing the issue of ignition of LSC and LSD waves. There are two principal mechanisms for the initial electron generation and growth: cascade ionization and multiphoton ionization (MPI). The first involves the absorption of laser radiation by electrons when they collide with neutrals (neutral IB). If the few initial electrons gain sufficient energy, they can impact ionize the gas or solid thereby leading to cascade breakdown in which the electron concentration will increase exponentially in time. For this process to occur there must be an initial electron in the focal volume and then the electrons must acquire an energy greater than the ionization potential of the gas. The second mechanism (MPI) involves the simultaneous absorption by an atom or molecule of a sufficient number of photons to cause its own ionization. This mechanism is more effective at shorter laser wavelengths, where the photons are more energetic. Both cascade and multiphoton ionization require high laser intensities, usually in excess of 10^8 W/cm^2. In solids, or in the presence of a solid surface, breakdown intensities as low as 10^6 W/cm^2 have been observed [11]. In transparent solids, this has been attributed to nonlinear self-focusing [11]. More frequently it can be related to microscopic absorption sites (typically impurities), a process termed thermal runaway.

IV. Modeling Thruster Processes

In this section, steady laser-heated flows are modeled [12]. A chemical equilibrium LSD wave model using LiH as a propellant is presented. Full details of this equilibrium model as well as the kinetic two-temperature model mentioned below are presented in [13]. The choice of this propellant is related to the low ionization potential of the LiH gas products and the relatively simple internal mode structure of these products. The structure of such LSD waves is derived. Extension to a two-temperature kinetic model [13] has also been implemented. The results of the two-temperature model are consistent with and validate the simpler equilibrium results. A schematic of the wave structure is given in Fig. 2. In this figure, region A represents the shock, and region B represents the absorption region. The LSD wave structure corresponds to $A + B$.

The stationary flow equations expressing conservation of mass, momentum, and energy in an inviscid, stationary

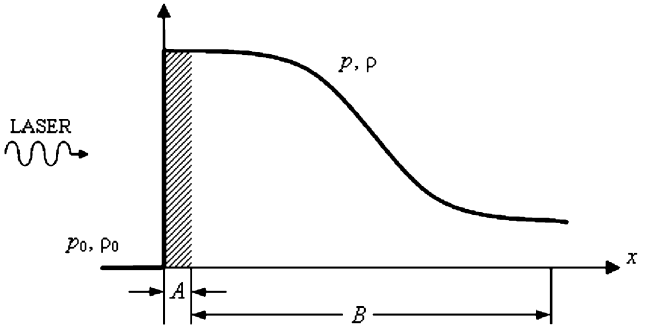

Fig. 2 Steady one-dimensional LSD wave.

quasi-one-dimensional gas in a duct in a reference frame traveling at the shock velocity D, relative to the laboratory, are given by [14,15]

$$\rho u A = \rho_0 u_0 A_0 \tag{3}$$

$$p + \rho u^2 = p_0 + \rho_0 u_0^2 \tag{4}$$

$$h + \tfrac{1}{2}u^2 = h_0 + \tfrac{1}{2}u_0^2 + q \tag{5}$$

In these equations $u = D - v$, while the heat absorbed by the gas per unit mass is $q = I_{\text{abs}}/\rho u$. I_{abs} is the absorbed laser power per unit area in any section. An ideal gas thermal equation of state and thermodynamic equilibrium is assumed. The duct section will be assumed constant throughout and heat fluxes through the wall are neglected. Absorption of laser radiation introduces a length scale into the problem and is given by

$$\frac{dI_{\text{abs}}}{dx} = k(I_0 - I_{\text{abs}}) \tag{6}$$

I_0 is the nominal laser intensity. In the k factor are included contributions from the different possible IB processes:

$$k = k_{e\text{LiH}} + k_{e\text{Li}} + k_{e\text{H}_2} + k_{e\text{H}} + k_{e\text{Li}^+} \tag{7}$$

The general expression for each of these contributions is different depending on whether one is dealing with charged (X^{Z+}) or neutral particles (X):

$$k_{eX^{Z+}} = \sigma_{eX^{Z+}} n_e n_{X^{Z+}} \left(e^{\frac{h_P v}{k_B T}} - 1\right), \qquad k_{eX} = \sigma_{eX} n_e n_X \left(1 - e^{\frac{h_P v}{k_B T}}\right) \tag{8}$$

Here n represents the number densities of the species involved. Subscripts e, Li, and H refer to electrons, lithium and hydrogen, respectively. The expressions used for the quantities σ are taken from Caledonia [16] to which the reader is referred.

The LSD wave structure for an incident intensity of 5 MW/cm^2 appears in Fig. 3. The total channel area is 1 cm^2. The gas is shocked at $x = 0$ and expands to the Chapman–Jouguet point with simultaneous absorption of laser radiation. Shocked conditions are determined for $I_{\text{abs}} = 0$. Absorption is calculated by forward

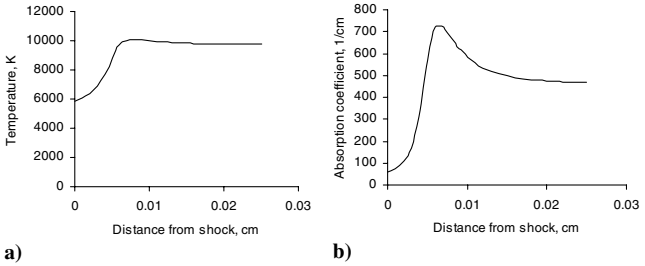

Fig. 3 LSD wave profiles for equilibrium LiH: a) temperature and b) absorption coefficient.

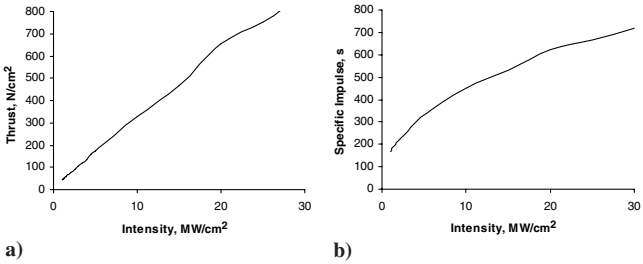

Fig. 4 Calculated property versus laser intensity: a) thrust and b) specific impulse.

integration of the system of Eqs. (3–5) in terms of the dimensionless density $\eta = \rho/\rho_0$ for decreasing η values until η_{CJ} is reached at which point the absorbed intensity is maximum, $I_{\text{abs}} = I_0$. The absorption coefficient at the Chapman–Jouguet point, k_{CJ}, is calculated as well as all the remaining thermodynamic variables. The spatial structure of the wave is then found by inverting Eq. (6). The initial conditions chosen are $v_0 = 0$ km/s, $p_0 = 4.70$ atm, $T_0 = 3000$ K, and $\rho_0 = 0.1$ kg/m^3. In the example, 99% of the laser radiation is absorbed in a 100 μm distance. The gas flow at the CJ point is at 10, 000 K with a pressure of about 37 atm. The particle speed is approximately 3.8 km/s. This heated flow generates thrust that can be further optimized by undergoing expansion through a nozzle. Although this simple model does not introduce a new calculational method, it does have the advantage of reproducing quite well the results of more complex two-temperature chemical kinetic calculations.

The results of a parametric variation of the intensity absorbed by a LSD wave and the consequent shock speed D and CJ particle quantities were used to compute thrust and specific impulse performance characteristics of a thruster using equilibrium LiH as a propellant. The cross sectional area of the flow is taken to be 1 cm^2. Figure 4 summarizes the results. The smallest value plotted, 1 MW, generates 44 N of thrust, corresponding to 4.4 kg of total mass for a thrust-to-weight ratio of 1. This represents but a lower bound as a ratio greater than 1 is required for an ascent. This one-dimensional thruster model generates low specific impulse (170 s) and has a mass flow rate of 25 (g/s)/cm^2. At this power level, the momentum coupling is high, 1175 (N/MW)/cm^2, and the energy density is approximately 40 MJ/kg. In this engine "chamber," only about 3% of the laser energy in the propellant is directed kinetic energy at this power level. Most of the energy is tied up in random kinetic temperature for conversion to thrust upon expansion through a nozzle. Experimental performance values under other conditions above 15% have been reported [17] and are expected to reach as much as 40% [18]. In this regard, the performance of this thruster chamber resembles a chemical thruster in terms of thrust and specific impulse.

Chemical thrusters are limited in specific impulse to at most 500 s with typical energy densities in the 4–6 MJ/kg range, but can reach as much as 12 MJ/kg. These examples serve to illustrate that in the laser propulsion thruster, energy densities roughly at least an order of magnitude higher than in chemical propulsion can be achieved. Because chemical energies are small in a relative sense, one cannot significantly improve laser thruster performance by using a more chemically energetic propellant. Improved performance requires higher laser powers or optimized pulse formatting in terms of pulse duration, pulse repetition frequency, and beam diffraction. In a more complete analysis, such improvements will, of course, be offset by losses such as viscous effects, radiation losses, and so on.

V. Flight Modeling of Laser Propulsion

Numerical simulations were performed to gain insight into the mechanics of laser propulsion ascent trajectories and how these are influenced by the most relevant mission parameters. The simulations were performed using COLVET [19]. This is a window application

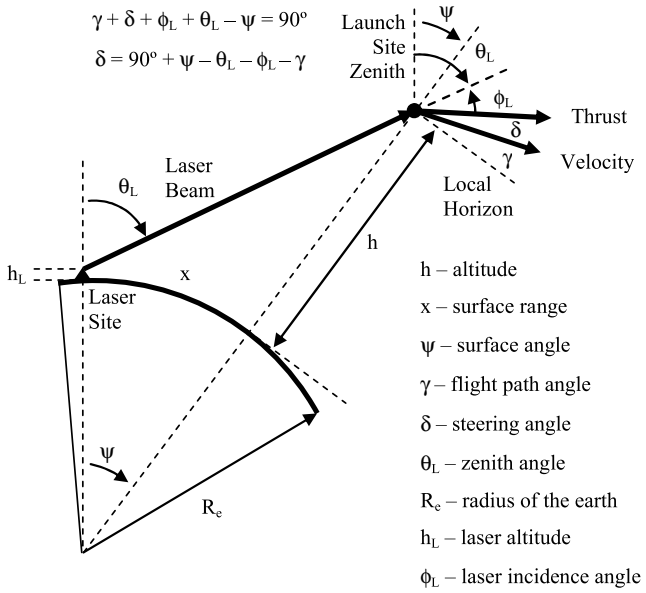

Fig. 5 Launch vehicle flight geometry (from Humble [20]).

coded in Fortran 95 incorporating object programming and a graphical user interface. The vehicle is assumed to be a point mass with the geometry depicted in Fig. 5 [20]. The position of the vehicle is given by the following equations, after integration using a Runge–Kutta algorithm [13]:

$$\begin{aligned}\ddot{r} &= F_r/m - r\dot{\Phi}^2 - r(\dot{\Lambda} + \Omega_e)^2\cos^2\Phi \\ \ddot{\Lambda} &= (1/r\cos\Phi)[F_\Lambda/m + 2\dot{r}(\dot{\Lambda} + \Omega_e)\cos\Phi + 2r\dot{\Phi}(\dot{\Lambda} \\ &\quad + \Omega_e)\sin\Phi] \\ \ddot{\Phi} &= (1/r)[F_\Phi/m - r(\dot{\Lambda} + \Omega_e)^2\sin\Phi\cos\Phi - 2\dot{r}\,\dot{\Phi}]\end{aligned} \tag{9}$$

These equations represent Newton's law. Accelerations appear on the left-hand side and the external forces F_r, F_Λ, and F_Φ appear on the right. All other terms on the right are a result of the coordinate transformations required to go from an inertial reference frame to the Earth-centered rotating reference frame. Each equation relates to each of the coordinates of this reference frame: radius, longitude, and latitude. Furthermore, as implicit in Eq. (9), there are no moments, that is, no rotational inertia. The only forces acting on the vehicle are gravity, aerodynamic drag, and propulsive thrust, which are added to produce the external force. The simulations take place over a spherical, nonrotating Earth, using the standard atmospheric model (International Standard Atmosphere).

The drag model is the same as in [19], with δ being the angle between the velocity vector and the thrust vector:

$$C_{\text{axial}} = 2\sin^2\theta_s + \sin^2\delta(1 - 3\sin^2\theta_s) \qquad C_{\text{norm}} = \sin 2\delta\cos^2\theta_s \tag{10}$$

The axial force coefficient C_{axial} is aligned with the longitudinal axis of the vehicle, whereas the normal force coefficient C_{norm} is perpendicular to it. This implies the vehicle must be a solid of revolution. The plane defined by the axial and normal force coefficients is the same as that defined by the velocity and thrust vectors. The latter is also parallel to the longitudinal axis of the vehicle, since there is no thrust vectoring. The fact that the simulation of the motion of a vehicle represented by a point-mass model has drag deserves comment. This is possible because the net external force in the point-mass equations can be the sum of any number of forces. The drag contribution is calculated based on the knowledge of the state of the vehicle: velocity (an inherently aerodynamic parameter), position (which corresponds to a certain atmospheric density), and attitude (which dictates the aerodynamic angles). The point-mass aspect of the simulation only relates to the motion of the vehicle. All other vehicle parameters can be modeled as pleased, as long as they are mathematically supported. The vehicle geometry was kept identical to that of [19], with the semivertex angle θs fixed at 55 deg.

Thrust is generated from a laser beam hitting the vehicle's "hot spot" following the law

$$F = \frac{2\eta_{\text{thr}}P_{\text{thr}}}{I_{\text{sp}}g_0} \tag{11}$$

Hot spot refers to the area of the vehicle that is illuminated by the laser and is, therefore, hot. It is in this area that the propellant is placed and ignited by the energy of the laser producing thrust. The thrust efficiency η_{thr} models losses in the conversion of the energy conveyed by the laser to propulsive power and is generally taken as 40% [18]. The received or propulsive power P_{thr} is the fraction of the initial laser power that reaches the vehicle

$$P_{\text{thr}} = \eta_{\text{atm}}\eta_{\text{diff}}P_{\text{lsr}} \tag{12}$$

The losses are mainly due to two factors: diffraction losses [20] and atmospheric absorption [20]

$$\eta_{\text{diff}} = 1\text{–}4\left(\Delta R_{\text{slant}}\frac{\lambda_{\text{lsr}}}{2\pi r_{\text{lsr}}r_{\text{hot spot}}}\right) \tag{13}$$

$$\eta_{\text{atm}} = \exp\left(-\alpha_{\text{abs}}(e^{-h_{\text{lsr}}/h_{\text{ref}}} - e^{-h/h_{\text{ref}}})\frac{h_{\text{ref}}}{\cos\theta_{\text{lsr}}}\right) \tag{14}$$

with $h_{\text{ref}} = 8$ km. An important parameter in laser propulsion that is used by the code is the laser intensity on the vehicle

$$I_{\text{lsr}} = \frac{P_{\text{thr}}}{\pi r_{\text{hot spot}}^2} \tag{15}$$

Benchmarking was performed with the purpose of increasing the confidence level in the results produced by COLVET. Two sorts of validations were performed: against available simulations in the literature [20] and against experimental results [21]. The validations performed aimed at reproducing as close as possible the same trajectory in COLVET as that of the validating sources, acknowledging that it is never possible to duplicate every single calculation, because different computer programs work inherently different. Moreover, laser-propelled launches depend heavily on the position of the vehicle, which naturally leads to the use of different control variables than used in traditional chemical rockets. A good example of this is the steering program, which in laser propulsion uses mostly the incidence angle (angle between the transmitted laser beam and the base of the vehicle) as opposed to the pitch angle (angle between the thrust vector and the local horizontal plane). Furthermore, several crucial parameters are simply not available. Again, the steering program is a good example. It is almost impossible to find data regarding the evolution of the attitude of the vehicle throughout the flight, which is irreplaceable when attempting a totally independent validation. Therefore, the trajectories were reproduced using a targeting or fitting strategy, which basically involves using the conventional pitch angle in simple evolutions (steps and slopes) to fit the resulting trajectory to that of the validating simulation.

Using a steering program, which is a curve relating the pitch or steering angle with time, with straight lines (hence steps and slopes) reduces the number of independent parameters needed to completely describe this curve. Another possibility would be to use, for example, a spline curve, which, however, would require a greater number of independent parameters for its definition. When targeting the simulation towards a reference trajectory, it becomes more practical to deal with a lower number of independent steering program parameters. It is important to realize that the steering program must be defined before the simulation starts (see Table 1 [13]). There exist other possibilities, but these would take us into the domain of control theory. It is important to note that the use of a steering program does not mean that the validation is biased or tampered. The steering

Table 1 Steering program for Humble and Pierson validation

Section	Time, s	Pitch, deg	Yaw, deg
1	130	90	270
2	44	45	270
3	35	−0.125 deg/s	90
4	50	Equal to end of Sec. III	90
5	177	−0.435 deg/s	90
6	38	0	90

Table 2 Humble and Pierson validation

	Humble & Pierson	COLVET	Error
Section I			
Altitude	27 km[a]	26.5 km	−1.9%
Section III			
Altitude	64 km[a]	69.4 km	8.4%
Ground range	23 km[a]	23.3 km	1.3%
Section IV			
Altitude	122 km[a]	116.1 km	−4.8%
Ground range	0 km	156 m	
Section V			
Altitude	300 km[a]	309.5 km	3.2%
Ground range	680 km[a]	642.5 km	−5.5%
Max vertical velocity	1700 m/s[a]	1458 m/s	−14.2%
Mass	400 kg	445 kg	11.25%
Time to orbit	449.5 s[a]	438 s	−2.6%
Flight path angle	0 deg	−0.33 deg	
Section VI			
Time		38 s	
Orbital velocity	7725 m/s	7642 m/s	−1.1%
End mass	400 kg	399.8 kg	−0.05%

[a]Data were read visually from plots.

program is merely a way of taking the vehicle over a certain trajectory. Certainly, if two trajectories are almost identical, both in space and time (i.e., similar velocity and acceleration profiles), the same can be said about their steering programs, but that misses the point. What is important is that the vehicle mass evolves in the same way in both simulations. Therefore, the criterion for a successful validation becomes the evolution of the combined set of state variables: position, velocity, acceleration, time, and mass. The validations against other simulations were quite satisfactory, Table 2 [13]. Validating simulation plots appear in [13]. The purpose of comparing a simulation with another is to ensure that the mathematical and physical models used to produce those simulations agree. An additional benefit is to build confidence in the simulation tool.

We next consider simulations on experimentally available data. Ground-breaking flight work on laser propulsion has been carried out by Leik Myrabo over the past few years [21]. The Lightcraft vehicle and mission details appear in Fig. 6 and Table 3, respectively.

An LSD wave is generated in the rear annular focal region of the concentrating optics. A ring of solid ablative propellant is placed in laser-sensitive areas. This vehicle uses both air and solid propellant as working fluids. Because of the lack of published information, some parameters were estimated. It is possible that the estimated parameters are not exactly those of the actual flight. However, given the agreement with the experimental results, any errors in the parameters seem to have canceled.

Figure 7 compares altitude and velocity with the data available in [21]. The simulation is remarkably close to experimental results. The vehicle reaches zero vertical velocity, exactly 12.7 s after launch at the hovering altitude of 71.3 m as reported in [21]. The initial acceleration phase, up to 2 s into the flight, is reproduced in the velocity profile. The altitude seems to be shifted vertically by a few meters but the linear evolution is mirrored. It may seem contradictory that the vehicle stops climbing while the laser continues to operate. The reason, as identified by the simulation (Fig. 8), is the diffraction efficiency, which is unintuitively low. The characteristic diffraction

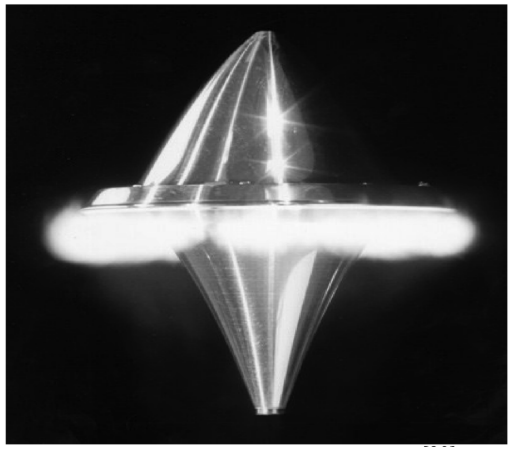

Fig. 6 Lightcraft vehicle [21].

length, the distance at which the laser power on the vehicle drops to zero due to diffraction is just about 90 m. Above this altitude there is no thrust. This may account for the lack of success that Myrabo encountered in taking his vehicles higher than 70 m. Drag is also of paramount importance. The peak drag amounts to about half of the available thrust. Had this vehicle been meant for higher velocities, it would need a more efficient aerodynamic shape. Thrust decreased monotonically as can be seen in the figure. Mass varied by 20% during the flight while the pitch angle and atmospheric absorption remained essentially constant.

Additional simulation under the conditions of Fig. 7 (or equivalently 8) but without diffraction show that indeed laser diffraction is height limiting; upon its elimination the vehicle will reach nearly 115 m in height, at which point thrust equals drag. Further height performance can still be achieved by optimizing vehicle drag.

Future experimental work should aim at taking a small vehicle, such as the one used by Myrabo, to several kilometers in altitude. Because that altitude will be most likely reached in a vertical ascent, the present analysis can be applied to this case. For the sake of clarity, this hypothetical flight will be called second-generation laser propulsion. The assumptions for this case are indicated in Table 4.

The vehicle is essentially identical to the first generation. The important difference is that the scale of the ascent is larger, at the expense of a tenfold increase in laser power and vehicle launch mass and widening the beam width a hundredfold to a meter. It is expected that even further increases in performance are attainable if the proper vehicle design is undertaken. One hundred kilowatt average power is currently the state of the art using CO_2 gas laser technology [22]. The concurrent optics is also available. The simulation results are summarized in the following plots (Fig. 9).

The mass consumption in the first-generation scenario was calculated at about 100 g; whereas for the second generation it amounts to about 2.36 kg. This mass is ablated material from the vehicle. An altitude of 8.04 km is reached in approximately 300 s. The velocity increase is sharp at the beginning of the flight, saturates, and decreases subsequently. Atmospheric transmission efficiency remains above 90%. However, the diffraction efficiency at maximum height is but one-third of its value at ground level. Thrust decreases monotonically from 9.6 N to about 2.6 N. At maximum velocity,

Table 3 Myrabo-like laser propulsion vehicle and laser

Launch mass	50.62	g	——
Diameter	12.2	cm	——
Laser power	10	kW	——
Laser wavelength	10.6	μm	——
Flight time	12.7	s	——
Drag coefficient	0.7	——	Estimated
Specific impulse	850	s	Estimated
Thrust efficiency	40%	——	Estimated
Main reflector diameter	1.0	cm	Estimated

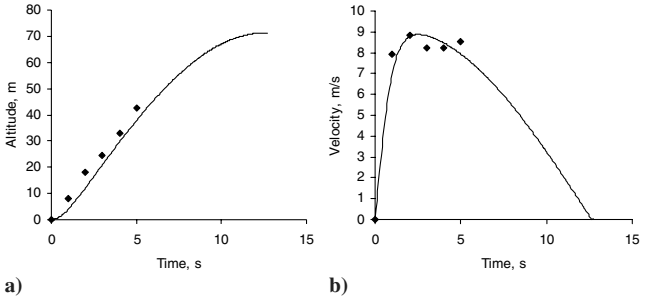

Fig. 7 Profile comparison with Myrabo flight results: a) altitude and b) velocity. Diamonds represent experimental data.

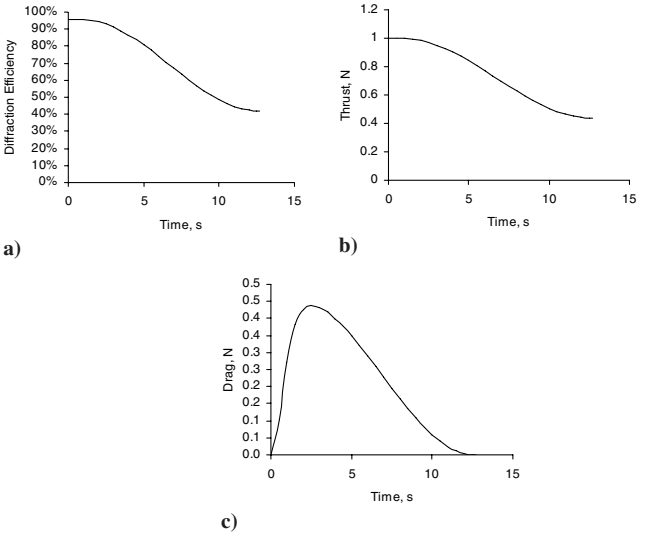

Fig. 8 Myrabo flight simulation results: a) diffraction coefficient, b) thrust, and c) drag.

thrust equals drag plus vehicle weight. The simulation indicates that laser flights to a few kilometers are possible with existing technology. Simulations were also performed for a low Earth orbit (LEO) launch. In this case, megawatt-class lasers are required to launch payloads of the order of 1 kg.

VI. Conclusions

The research reported here presents the main results of a more extensive investigation into laser propulsion [13]. For a ground launch, only a thermal thruster concept is viable. Full advantage of laser propulsion requires that higher specific energies be deposited in the propellant. Of the thermal concepts/technologies studied, the most promising is the LSD wave mechanism, either the air breathing or rocket mode. The LSD generates higher I_{sp} and higher thrust as compared to the LSC combustion mode. Although not discussed herein, a natural extension of this work for enhancing thermal system performance is to investigate pulse formatting. A combination of short pulses, up to the 10^{-9} s range, and high repetition rates, in the 10^4–10^5 Hz range, may lead to substantially improved thruster performance.

The LSD mechanism, and quite generally other plasma absorption mechanisms, require prompt uniform ignition. This can be achieved either by laser focusing or by using a low temperature ionization

Table 4 Second generation of Myrabo-like laser propulsion

Launch mass	500	g
Target altitude	8	km
Laser power	100	kW
Main reflector diameter	100	cm

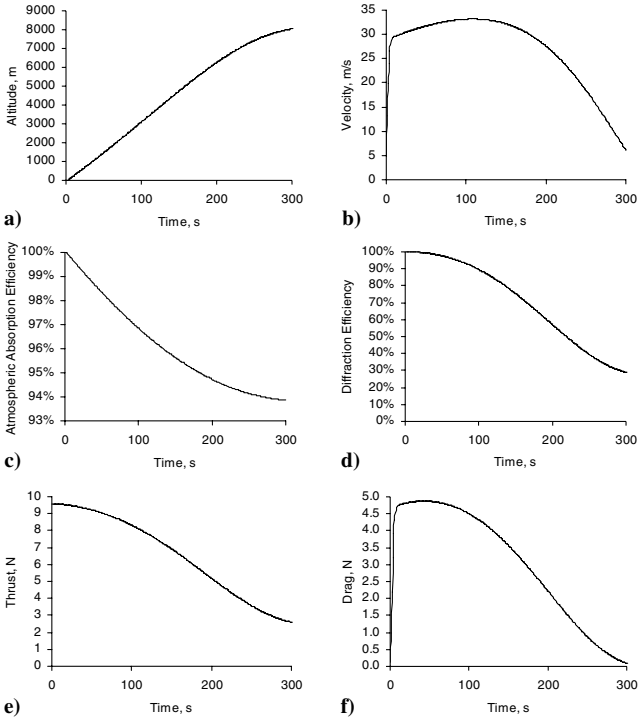

Fig. 9 Second-generation Myrabo-like laser propulsion: a) altitude; b) velocity; c) atmospheric absorption efficiency; d) diffraction efficiency; e) thrust; f) drag.

mechanism. Within a narrow range of specific enthalpy, it may prove advantageous to use a noble gas, such as He, as a propellant along with a low ionization potential seed. In this way, the absorbed laser energy would be deposited in the translational modes (pressure) of the propellant minimizing internal energy deposition. The associated laser intensity window for laser propulsion is limited to 10^6 W/cm^2 from below (ignition threshold) and 10^{11} W/cm^2 from above (atmospheric propagation limit).

To protect walls from the high temperatures reached, in the 10,000–20,000 K range, it is important to use ablative material on sensitive surfaces. Laser beam steering for laser propulsion is very complex and technologically demanding and deserves separate treatment. A viable alternative to steering uses passive stabilization in which the launch vehicle "searches" for the laser beam. This concept has been termed "beam riding." The thruster should be designed so that axial deviations are stabilized by the propellant flow configuration. Transverse stabilization can be achieved by requiring that the center of thrust be ahead of the center of drag.

From ballistics considerations alone, there is a minimal laser power that will launch a given mass. Small vehicles have limited launch ranges due to drag effects. Aerodynamic design should be a major design driver. Current available state-of-the-art laser power levels, of the order of 100 kW in CW mode for CO_2 lasers, will allow launching of 200 g in mass to above 10 km in height. For flights to LEO, preliminary simulations with COLVET indicate that the minimal size is 3 kg using a 3 MW laser.

Acknowledgment

The authors acknowledge the financial support of the European Space Agency (ESA) through contract 17048/03/NL/PA "Laser Propulsion for ESA Missions: Ground to Orbit Launch."

References

[1] Johnson, R. O., Dymchits, B. M., Ivanov, G. V., Mescherskiy, A. N., Reilly, J. P., and Lander, M. L. "Laser-Material Test Results from Russian High Power Carbon Monoxide Laser," *Proceedings of SPIE*, Vol. 2714, SPIE–International Society for Optical Engineering, Bellingham, WA, 1996, pp. 222–228.

[2] Williams, F., *Combustion Theory* 2nd ed., Benjamin Publishing Company, Menlo Park, CA, 1985.
[3] Kemp, N. H., and Krech, R. H., "Laser-Heated Thruster Final Report," NASA CR-161665 (PSI TR-2220), Physical Sciences, Inc., Andover, MA, Sept. 1980.
[4] Legner, H. H., and Douglas-Hamilton, D. H., "CW Laser Propulsion," *Journal of Energy*, Vol. 2, March–April 1978, pp. 85–94.
[5] Wu, P. K. S., and Pirri, A. N., "Stability of Laser-Heated Flows," *AIAA Journal*, Vol. 14, March 1976, pp. 390–392.
[6] Pirri, A. N., Root, R. G., and Wu, P. K. S., "Plasma Energy Transfer to Metal Surfaces Irradiated by Pulsed Lasers," *AIAA Journal*, Vol. 16, No. 12, 1978, pp. 1296–1304.
[7] Boni, A. A., Su, F. Y., Thomas, P. D., and Tusal, H. M., "Theoretical Study of Laser-Target Interactions," Science Applications Inc., Mid-Term TR SAI 76-722-LJ, La Jolla, CA, Aug. 1976.
[8] Pirri, A. N., "Analytic Solutions for Laser-Supported Combustion Wave Ignition Above Surfaces," AIAA Paper 76-23, Washington, D.C., Jan. 1976.
[9] Rosen, D. L., Kemp, N. H., Weyl, G., Nebolsine, P. E., and Kothandaraman, R., "Pulsed Laser Propulsion Studies Vol I, Thruster Physics and Performance," Physical Sciences Inc. PSI TR-184, Andover, MA, 1982.
[10] Caledonia, G. E., Wu, P. K. S., and Pirri, A. N., "Radiant Energy Absorption Studies for Laser Propulsion," NASA CR-134809 (PSI TR-20), Physical Sciences, Inc., Andover, MA, March 1975; see also *Journal of Energy*, Vol. 1, March–April 1977, pp. 121–124.
[11] Measures, R. M., and Cardinal, P. G., "Laser Ionization Based on Resonance Saturation: A Simple Model Description," *Physical Review A*, Vol. 23, No. 2, 1981, pp. 804–815.
[12] Weyl, G., Rollins, C., and Resendes, D., "Structure and Maintenance Threshold of Laser Supported Detonation Waves," *Proceedings of the 17th Annual Shock Tube Symposium*, edited by Y. Kim, AIP Conference Proceedings 208, Current Topics and Shock Waves, AIP, New York, July 1989, pp. 365–370.
[13] Resendes, D. P., Mota, S., Sorasio, G., Mendonça, J. T., Sanders, B., and Encarnação, J., "Laser Propulsion for ESA Missions: Ground to Orbit Launch," ESA CR 17048/03/NL/PA, Dec. 2004 (Distribution: Public).
[14] Pirri, A. N., Monsler, M. J., and Nebolsine, P. E., "Propulsion by Absorption of Laser Radiation," *AIAA Journal*, Vol. 12, No. 9, Sept. 1974, pp. 1254–1261.
[15] Simons, G. A., and Pirri, A. N., "The Fluid Mechanics of Pulsed Laser Propulsion," *AIAA Journal*, Vol. 15, No. 6, June 1977, pp. 835–842.
[16] Caledonia, G. E., Wu, P. K. S., and Pirri, A. N., "Radiant Energy Absorption Studies for Laser Propulsion," NASA CR-134809 (PSI TR-20), Physical Sciences, Inc., Woburn, MA, March 1963.
[17] Rollins, C., Bailey, A., Gelb, A., Resendes, D., and Weyl, G., "Evaluation of Laser Supported Detonation Wave Thrusters from Ground to Orbit Launch," AIAA Paper 89-1914, 1989.
[18] Kantrowitz, A., "Propulsion to Orbit by Ground Based Lasers," *Astronautics and Aeronautics*, Vol. 10, No. 5, 1972, pp. 74–76.
[19] Encarnação, J., "Numerical Simulations of Ascent Trajectories," Masters Thesis, Delft Aerospace, University of Delft, 2005.
[20] Humble, W. E., and Pierson, B. L., "Maximum-Payload Trajectories for a Laser-Propelled Vehicle," *Journal of Guidance, Control, and Dynamics*, Vol. 18, No. 6, 1995, pp. 1259–1266.
[21] Myrabo, L. N., "Brief History of the Lightcraft Technology Demonstrator (LTD) Project," *1st International Symposium on Beamed Energy Propulsion*, edited by A. Pakhomov, AIP Conference Proceedings No. 664, AIP, New York, 2002, pp. 49–60.
[22] Rodin, A. V., Naumov, V. G., Nastoyashchii, A. F., and Shashkov, V. M., "High Energy Pulse-Repetitive CO2 Laser for Lightcraft Experiments," *1st International Symposium on Beamed Energy Propulsion*, edited by A. Pakhomov, AIP Conference Proceedings 664, AIP, New York, 2002, p. 612.

A. Gallimore
Associate Editor